

Enhanced X-Ray Angular Dispersion and X-ray Spectrographs with Resolving Power Beyond 10^8

Yuri Shvyd'ko^{1,*}

¹*Advanced Photon Source, Argonne National Laboratory, Argonne, Illinois 60439, USA*

Spectrograph is an optical device that is used to disperse photons of different energies E into distinct directions and space locations, and to take a snapshot of the whole spectrum of photon energies with a spatially sensitive photon detector. Substantial advantage of a spectrograph over an ordinary spectral analyzer, is its ability to deal with many photon energies simultaneously, thus reducing exposure time per spectrum considerably. To realize a spectrograph, dispersing elements with large angular dispersion rate are required. Here we show, on the example of CDW x-ray optics [1–3], that multi-crystal arrangements may feature cumulative angular dispersion rates more than an order of magnitude larger than those attainable in single Bragg reflections. This makes, first, hard x-ray spectrographs feasible, and, secondly, a resolving power beyond $E/\Delta E \gtrsim 10^8$ achievable.

PACS numbers: 41.50.+h, 07.85.Nc, 61.10.-i, 78.70.Ck

Spectrograph is capable of measuring simultaneously a spectrum of photon energies E , and therefore is an optical device more desirable than an ordinary spectral analyzer, that measures energy of a single photon at a time. Spectrographs are especially wanted when long exposures (data collecting time) are required. This is always the case, if a very high resolving power is involved and the light sources are not especially bright. High-resolution spectroscopies in hard x-ray regime, which are used to study atomic dynamics and electronic excitations, is the realm where spectrographs would be extremely favorable due to mentioned constraints. Here we show that angular dispersion of hard x-rays can be enhanced by more than an order of magnitude in multi-crystal arrangements, and this effect can be used to realize spectrographs in hard x-ray regime. Notably, the spectrographs become feasible with a resolution power of $E/\Delta E \gtrsim 10^8$, what may advance significantly research using high-resolution x-ray spectroscopies, in particular inelastic x-ray scattering.

Czerny-Turner [4] grating spectrographs are nowadays standard in infrared, visible, and ultraviolet spectroscopies [5, 6]. In its classical arrangement, the Czerny-Turner spectrographs comprise a few elements shown schematically in Fig. 1: first, a collimating mirror M_C , which collects photons from a radiation source S and makes the photon beam parallel, secondly, a dispersing element DE such as diffraction grating or a prism, which disperses photons of different photon energies into different directions, thirdly, a curved mirror M_F which focuses photons of different energies into different locations $F(E)$, and, last but not least, a spatially sensitive photon detector Det placed in the focal plane to record the whole photon spectrum. To achieve high resolution, what matters most, is the magnitude of the angular dispersion rate $\mathcal{D} = \delta\theta'/\delta E$, which measures the variation of the reflection angle θ' with photon energy E upon reflection from the dispersing element. For a given path-length L ($DE \rightarrow M_F \rightarrow Det$) from the dispersing element to the source image $F(E)$ on the detector, the angular disper-

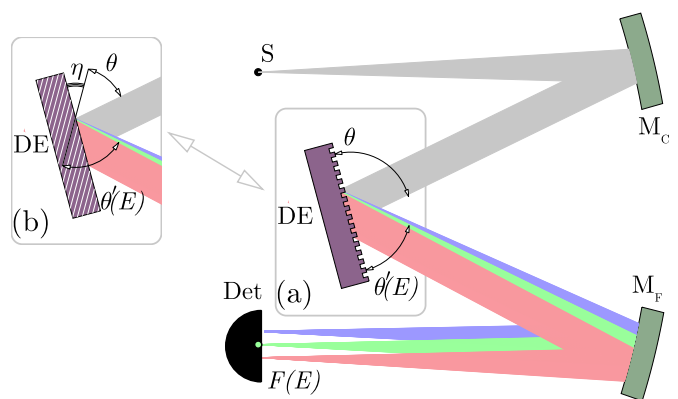


FIG. 1: Scheme of the Czerny-Turner type [4] spectrograph with diffraction grating (a), or a crystal in asymmetric Bragg diffraction (b) as dispersing element DE . Other components include radiation source S , collimating and focusing mirrors M_C and M_F , and position sensitive detector Det .

sion rate \mathcal{D} determines the magnitude of the source image position variation with photon energy $\delta F(E) = \mathcal{D}L \delta E$. In the following, $\mathcal{D}L$ is termed spatial dispersion. The smallest spectral interval ΔE between spectral components, which can be resolved is therefore

$$\Delta E = \frac{1}{\mathcal{D}} \frac{\Delta F}{L}, \quad (1)$$

where ΔF is the smallest of the two values, either source S image size on the detector for a particular monochromatic component, or detector spatial resolution.

Nowadays, diffraction grating manufacturing technology has advanced to the extent, that grating spectrographs are being successfully used with much shorter wavelengths, in particular in soft x-ray regime ($\lesssim 1$ keV) [7, 8] attaining resolving power of $E/\Delta E \simeq 10^4$. Extension into the hard x-ray regime is, however, not trivial, because of the lack of hard x-ray optics elements with sufficiently large dispersion rate.

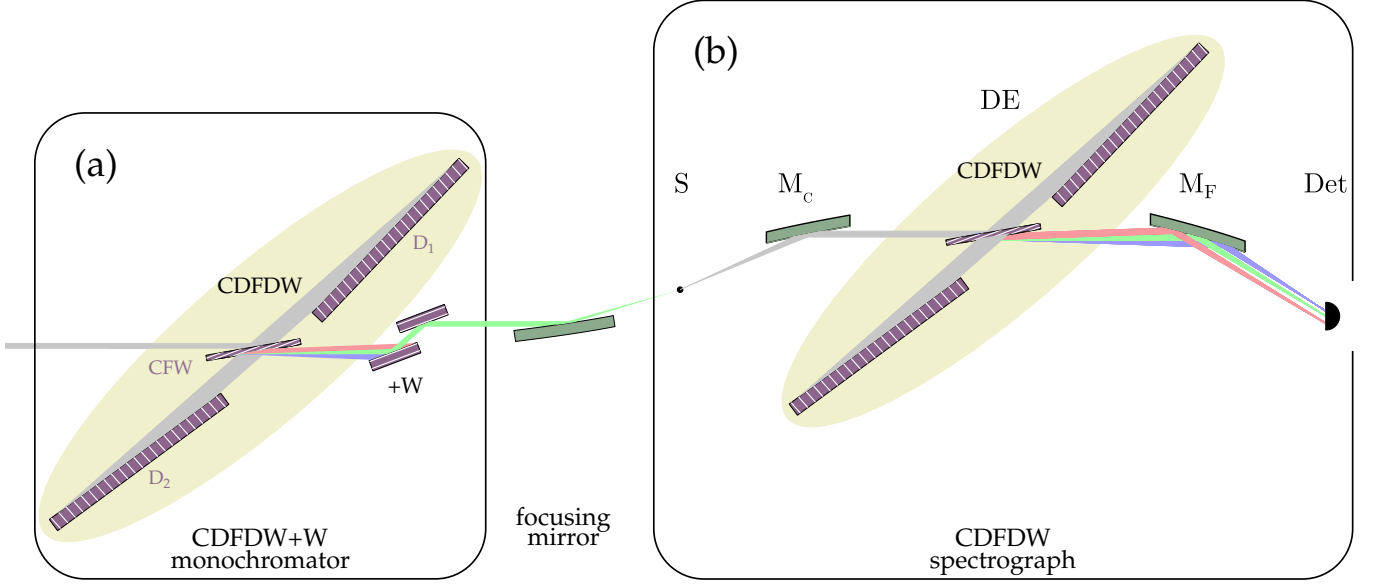


FIG. 2: Layout of an inelastic x-ray scattering (IXS) instrument consisting of an x-ray monochromator (a), focusing mirror, and an x-ray spectrograph (b). The x-ray monochromator (a) consists of a CDFDW three-crystal (CFW, D_1 , D_2) optics and supplementary wavelength selector +W. The x-ray spectrograph (b), of Czerny-Turner type, uses the CDFDW optics as dispersing element DE (compare Fig. 1).

A hard x-ray equivalent of the optical diffraction grating is an asymmetrically cut crystal with reflecting atomic planes at non-zero asymmetry angle $\eta \neq 0$ to the crystal face, as shown schematically in Fig. 1(b). In Bragg diffraction from asymmetrically cut crystals angular dispersion of x-rays takes place [1, 2, 9, 10]. A collimated x-ray beam at a glancing angle of incidence θ to the reflecting atomic planes, is fanned-out upon reflection with photons of different energies propagating at different angles $\theta'(E) \neq \theta$, with a dispersion rate

$$\mathcal{D} = \frac{2}{E} \frac{\sin \theta \sin \eta}{\sin(\theta - \eta)} = \frac{|b| + 1}{E} \tan \theta \xrightarrow{\theta \rightarrow 90^\circ} \frac{2 \tan \eta}{E}. \quad (2)$$

Here, $b = -\sin(\theta + \eta)/\sin(\theta - \eta)$ is the asymmetry parameter. Dispersion rates of $\simeq 8 - 12 \mu\text{rad}/\text{meV}$ were demonstrated in Bragg diffraction from strongly asymmetrically cut crystals ($\theta - \eta \simeq 2^\circ$) close to exact back scattering ($\theta \simeq 90^\circ$) where \mathcal{D} is maximal [2, 3].

The effect of angular dispersion can be used to monochromatize x-rays beyond the limits determined by the spectral width of Bragg reflections [1, 2]. This can be accomplished by using a CDW type optics with three key elements: a collimator (C), dispersing element (D) and wavelength selector (W) [1, 11]. Asymmetrically cut crystals are used as C, D, and W elements. In particular, demonstrated recently an advanced CDW scheme, CDFDW monochromators [3], can monochromatize to bandwidths $\Delta E_\Sigma = 0.5 \text{ meV}$ and less, achieving a resolving power of $E/\Delta E_\Sigma \gtrsim 10^7$ at $E = 9.1 \text{ keV}$.

The use of asymmetrically cut crystal as dispersing ele-

ment was proposed for a “focusing monochromator” [12]. The crystal is combined with a focusing x-ray lens which Fourier transforms angular dispersion into spatial dispersion. As was correctly noticed in [12] such optics can be used as a monochromator, however, not as a spectral analyzer (or spectrograph), as a small angular size of the radiation source is required for its realization.

As Fig. 1 suggests, the x-ray spectrograph can be realized by substituting the diffraction grating in the Czerny-Turner scheme by an asymmetrically cut crystal. However, the mentioned above practically achievable dispersion rate in single Bragg reflection $\mathcal{D} \simeq 10 \mu\text{rad}/\text{meV}$ is barely useful, since only with path lengths $L \gtrsim 10 \text{ m}$ a reasonably large spatial dispersion rate of $L\mathcal{D} \gtrsim 100 \mu\text{m}/\text{meV}$ can be attained. Here we show, on the example of CDW x-ray optics [1–3], that multi-crystal arrangements may feature cumulative angular dispersion rates more than an order of magnitude larger than those attainable in single Bragg reflections - Eq. 2. It is this enhanced cumulative angular dispersion rate that makes hard x-ray spectrographs feasible.

We will use the CDFDW optics [3], an advanced CDW scheme, as an example, to demonstrate how the enhanced cumulative angular dispersion rate appears in multi-crystal arrangements. The CDFDW optics, shown schematically inside the shaded oval area of Fig. 2(a), consists of three crystals: CFW, D_1 , and D_2 executing five successive Bragg reflections. Each of the five reflection has its own key function termed as C (collimator), D (dispersing element), F (anomalous transmission filter), D, and W (wavelength selector) respectively. For a de-

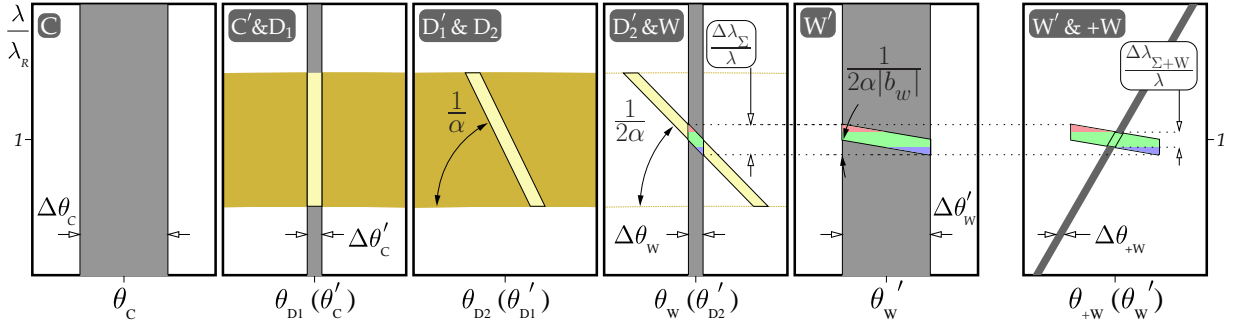


FIG. 3: DuMond diagrams for the sequence of Bragg reflections from elements of the CDFDW+W optics - Fig. 2(a). Gray and brown stripes are regions of Bragg reflections in the space of x-ray wavelengths λ and angles of incidence θ_H or reflection θ'_H from the optical elements ($H=C, D_1, D_2, W$, and $+W$). D-element is set into backscattering ($\theta_D \rightarrow \pi/2$) with the center of the reflection spectral range at λ_R . Yellow stripes display the overlapping reflection regions of the C- and D-elements. Tricolor tetragons display the reflection region common for all elements of the CDFDW optics. Green tetragon in $W' \& +W$ shows reflection region common for all elements of the CDFDW+W optics

tailed discussion of the principles of the CDFDW optics, we refer to [3]. Here, we use DuMond diagram analysis [13] to calculate the angular acceptance $\Delta\theta_\Sigma$ for the input radiation, angular spread $\Delta\theta'_\Sigma$ and spectral bandwidth for the output radiation ΔE_Σ , but most importantly the dispersion rate after each Bragg reflection, and the cumulative dispersion rate \mathcal{D}_Σ of entire optics. Figure 3 shows DuMond diagrams for the sequence of all Bragg reflections, except for the anomalous transmission through the CFW crystal (F-reflection). This omission does not change substantially main results of the analysis.

Gray and brown stripes are the regions of Bragg reflections in the space of x-ray wavelengths λ and angles of incidence θ_H or reflection θ'_H from the crystals in one of the reflections $H=C, D_1, D_2$, or W . All the crystals are asymmetrically cut with asymmetry angle η_H . The yellow stripes display the overlapping reflection regions of the C- and D-crystals. Tricolor tetragons display the reflection region common for all elements. D-element is set into backscattering ($\theta_D \rightarrow \pi/2$) with the center of the reflection spectral range at λ_R .

The asymmetry parameter of the CFW crystal in the C-reflection, has to be chosen small $|b_C| \ll 1$ to accept incident photons in a broad angular range $\Delta\theta_C$ and collimate them into a beam with a small divergence $\Delta\theta'_C$:

$$\Delta\theta_C = \Delta\theta_C^{(s)}/\sqrt{|b_C|}, \quad \Delta\theta'_C = \Delta\theta_C^{(s)}/\sqrt{|b_C|}. \quad (3)$$

For a low indexed Bragg reflection, such as Si(220), the angular width in symmetric reflection geometry $\Delta\theta_C^{(s)} \simeq 23 \mu\text{rad}$. By choosing $|b_C| = 1/21.5$, as in [3], the angular acceptance of the C-element, as well as of the entire CDFDW optics, becomes large $\Delta\theta_C = 106 \mu\text{rad}$, while the angular spread of x-ray impinging on D_1 crystal - small: $\Delta\theta'_C = 5 \mu\text{rad}$. The phase space for C-reflection is shown in diagrams C and $C' \& D_1$, as stripes almost vertical due to a small Bragg angle $\simeq 20.8^\circ$. Yellow strip indicates the common phase space for photons upon both

reflections C- and D_1 . In diagram $D'_1 \& D_2$, it is shown rotated by an angle $\arctan(1/\alpha)$, where $\alpha = 2 \tan \eta_D$ - Eq. (2) - due to angular dispersion upon reflection D'_1 . Reflection D_2 doubles the dispersion rate to $4 \tan \eta_D$, indicated by the larger inclination of the phase space in diagram $D'_2 \& W$. Only those photons are reflected from the CFW crystal in the W-reflection, which are concentrated in the small angular range of the W-reflection $\Delta\theta_W = \Delta\theta_W^{(s)}/\sqrt{|b_W|} = \Delta\theta'_C$. Here $|b_W| = 1/|b_C| = 21.5 \gg 1$. The W-reflection selects photons in a small angular range, and most importantly in a bandwidth much smaller than the bandwidth of the D-reflections:

$$\frac{\Delta E_\Sigma}{E} = \frac{\Delta\lambda_\Sigma}{\lambda} = \frac{\Delta\theta'_C + \Delta\theta_W}{4 \tan \eta_D} = \frac{\Delta\theta_W}{2 \tan \eta_D}. \quad (4)$$

Remarkably, the photons are spread upon the W-reflection into a large angle, which is equal to the angular acceptance of the CDFDW optics

$$\Delta\theta'_\Sigma = \Delta\theta_\Sigma = \Delta\theta_W^{(s)}\sqrt{|b_W|} = \Delta\theta_C^{(s)}/\sqrt{|b_C|}, \quad (5)$$

within the accuracy of the DuMond diagram analysis.

Here we are arriving at the crucial point. From diagram W' in Fig. 3, it follows, that the W-reflection not only increases the beam divergence, it also increases by the same factor of $|b_W|$ the tangent of the phase space, i.e. it increases the angular dispersion rate from $2\mathcal{D}$ to

$$\mathcal{D}_\Sigma = 2\mathcal{D}|b_W| = \frac{4 \tan \eta_D}{E} |b_W|. \quad (6)$$

That means that the cumulative angular dispersion rate \mathcal{D}_Σ , the CDFDW optics endowed with, is by a factor of $\simeq |b_W|$ greater than the largest dispersion rate \mathcal{D} achievable in single Bragg reflection. In the example of [3], $\eta_D = 88^\circ$, $\mathcal{D} = 6.3 \mu\text{rad}/\text{meV}$, $|b_W| \simeq 21.5$, and therefore $\mathcal{D}_\Sigma = 270 \mu\text{rad}/\text{meV}$. The dispersion rate enhancement is large $\mathcal{D}_\Sigma/\mathcal{D} \gtrsim 40$, and can be used at least twofold.

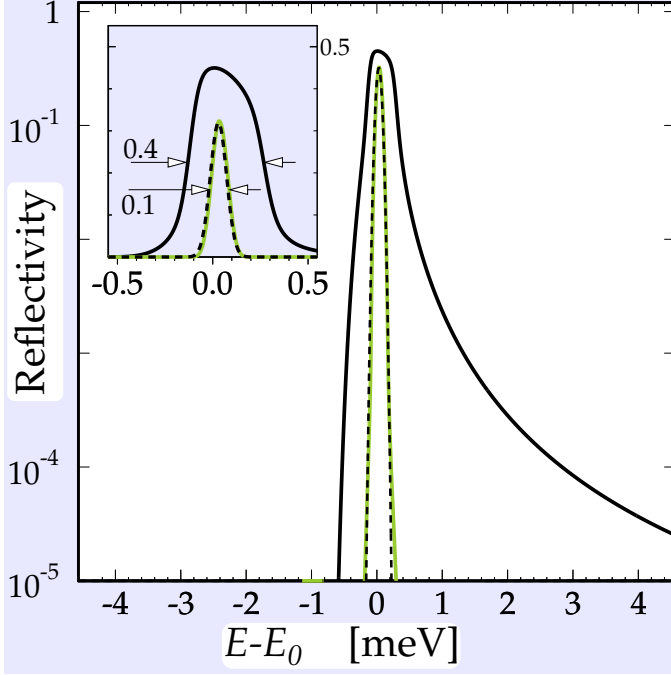


FIG. 4: Dynamical theory calculations of the spectral distribution of x rays after five successive reflection in the CDFDW optics (black line) and after additional two reflections from the supplementary wavelength selector +W (green line). Black dashed line shows Gaussian distribution of the same full width at half maximum. Inset shows the same distributions on the linear scale. The Bragg reflections and crystal parameters are used for the CDFDW optics the same as in [3]. The Si(220) reflection in symmetric geometry is chosen for +W.

First, the bandwidth of the CDFDW monochromator can be further reduced by applying one more Bragg reflection with an angular width $\Delta\theta_{+w} \ll \Delta\theta'_w$, see Fig. 3(W'+W). To keep the beam direction unchanged, a better choice is two equivalent Bragg reflections from crystals in non-dispersive configuration, as shown schematically in Fig. 2(a), and denoted by +W for supplementary wavelength selector. Figure 4 shows dynamical theory calculations for +W as Si crystals in the (220) Bragg reflection in symmetric geometry, other parameters of the CDFDW optics equivalent to those realized in [3], and a $20 \mu\text{rad}$ angular spread for incident photons. The application of the supplementary wavelength selector reduces the bandwidth from 0.4 meV to 0.1 meV, what correlates with the estimation using the DuMond diagram W'+W. However, not only the +W-reflections reduce the bandwidth, they make the wings of the spectral distribution extremely sharp, as sharp as of the Gaussian distribution. With smaller $\Delta\theta_{+w}$ the bandwidth can be further reduced.

Secondly, the large dispersion rate enhancement can be used to realize a hard x-ray spectrograph. Its scheme is shown in Fig. 2(b), as a part of an IXS instrument,

comprising also the CDFDW+W monochromator and a 2D-mirror focusing x-rays on sample S. The CDFDW spectrograph is similar to the Czerny-Turner spectrograph presented in Fig. 1, with one major difference. The diffraction grating (or the single crystal) is substituted by a multi-crystal optics with enhanced dispersion rate. The components of the spectrograph are also almost equivalent to the components of the CDW analyzer proposed in [1] (Sec. 6.3). The crucial difference is that the 2D-focusing mirror M_F is added downstream the multi-crystal optics. This converts the analyzer into a spectrograph with potentially much higher spectral resolution. If mirrors M_C and M_F are equivalent and perfect, the system produces 1:1 image of the source S (x-ray scattered from sample S) on the detector Det with monochromatic x-rays independent of the distances between the mirrors and the distances of the CDFDW optics to the mirrors. On the other hand, the path-length L from the CDFDW optics to the source image scales the linear dispersion rate $\mathcal{D}_\Sigma L$.

The cumulative dispersion rate of the CDFDW optics studied in [3] is $\mathcal{D}_\Sigma = 270 \mu\text{rad}/\text{meV}$. This results in a large linear dispersion rate $\mathcal{D}_\Sigma L = 270 \mu\text{m}/\text{meV}$, even with a reasonably small $L \simeq 1 \text{ m}$. L can be increased without degrading the source image size ΔF . The resolution of the spectrograph is limited, according to Eq. (1) by ΔF . Assuming the sources size to be $\simeq 5 - 10 \mu\text{rad}$, as discussed in [1] (Sec. 6.3), $\Delta F \lesssim 50 \mu\text{m}$ is feasible, also if some broadening due to figure errors in mirrors are involved. Therefore $\Delta E_\Sigma \lesssim 0.1 \text{ meV}$, and resolving power $E/\Delta E_\Sigma \gtrsim 10^8$ is feasible.

The DuMond diagram analysis presented in Fig. 3 suggests, that the enhanced cumulative dispersion rate appears in multi-crystal optics if a wavelength selector is applied as asymmetrically cut crystal with $|b_w| \gg 1$. This property is general. It is not a unique feature of the CDW-type crystal optics. The (+, -, -, +) monochromator composed of four asymmetrically cut crystals [14], is another example. Using the results of the DuMond diagram analysis presented in Sec. 3.5 of [1] by Eqs. (3.32)-(3.33), it is easy to show that the cumulative angular dispersion rate of the (+, -, -, +) monochromator $\mathcal{D}_\Sigma \propto \Delta\theta'/\Delta E \simeq \tan\theta|b_3 b_4|/E$, where $|b_n| \gg 1$ is the absolute value of the asymmetry parameter for the 3rd and 4th Bragg reflection. The dispersion rate for a single reflection is $\mathcal{D} \propto \tan\theta(|b_3| + 1)/E$, according to Eq. (2). Therefore, cumulative \mathcal{D}_Σ is enhanced by a factor of $|b_4|$.

In conclusion, multi-crystal x-ray optics with crystals in asymmetric diffraction may exhibit enhanced cumulative dispersion rate, more than an order of magnitude larger than the dispersion rate associated with a single Bragg reflection. Such optics can be used as dispersing element in Czerny-Turner-type x-ray spectrographs. Czerny-Turner-type spectrograph with CDW dispersing optics may feature resolving power beyond 10^8 . Czerny-Turnerscheme could be also used to realized

high-resolution spectrographs in soft x-ray regime.

S. Stoupin is acknowledged for reading the manuscript and valuable suggestions. Work was supported by the U.S. Department of Energy, Office of Science, Office of Basic Energy Sciences, under Contract No. DE-AC02-06CH11357.

* Electronic address: shvyd'ko@aps.anl.gov

- [1] Shvyd'ko, Yu. *X-Ray Optics – High-Energy-Resolution Applications*, vol. 98 of *Optical Sciences* (Springer, Berlin Heidelberg New York, 2004).
- [2] Shvyd'ko, Yu. V. *et al.* Bragg diffraction of x rays in asymmetric backscattering geometry. *Phys. Rev. Lett.* **97**, 235502 (2006).
- [3] Shvyd'ko, Yu., Stoupin, S., Shu, D. & Khachatryan, R. Using angular dispersion and anomalous transmission to shape monochromatic x rays. *Phys. Rev. A (accepted)*, eprint *arXiv:1108.2487* (2011).
- [4] Czerny, M. & Turner, A. F. Über den Astigmatismus bei Spiegelspektrometern. *Z. f. Physik* **61**, 792–797 (1930).
- [5] Shafer, A. B., Megill, L. R. & Droppelman, L. Optimization of the Czerny-Turner Spectrometer. *J. Opt. Soc. Am.* **54**, 879–886 (1964).
- [6] Lee, K.-S., Thompson, K. P. & Rolland, J. P. Broadband astigmatism-corrected Czerny-Turner spectrometer. *Opt. Express* **18**, 23378 – 23384 (2010).
- [7] Ghiringhelli, G. *et al.* SAXES, a high resolution spectrometer for resonant x-ray emission in the 400-1600 eV energy range. *Rev. Sci. Instrum.* **77**, 113108 (2006).
- [8] Braicovich, L. *et al.* Magnetic excitations and phase separation in the underdoped $\text{La}_{2-x}\text{Sr}_x\text{CuO}_4$ superconductor measured by resonant inelastic x-ray scattering. *Phys. Rev. Lett.* **104**, 077002 (2010).
- [9] Kuriyama, M. & Boettinger, W. J. On the angular divergence of out-going beams in an asymmetric diffraction geometry. *Acta Cryst.* **A32**, 511 (1976).
- [10] Brauer, S., Stephenson, G. & Sutton, M. Perfect crystals in the asymmetric bragg geometry as optical elements for coherent x-ray beams. *J. Synchrotron Rad.* **2**, 163–173 (1995).
- [11] Shvyd'ko, Yu. V. *et al.* Progress in the development of new optics for very high resolution inelastic x-ray scattering spectroscopy. *AIP Conf. Proc.* **879**, 737–745 (2007).
- [12] Kohn, V. G., Chumakov, A. I. & Rüdfer, R. Wave theory of focusing monochromator of synchrotron radiation. *J. Synchrotron Rad.* **16**, 635–641 (2009).
- [13] DuMond, J. W. M. Theory of the use of more than two successive x-ray crystal reflections to obtain increased resolving power. *Phys. Rev.* **52**, 872–883 (1937).
- [14] Yabashi, M., Tamasaku, K., Kikuta, S. & Ishikawa, T. An x-ray monochromator with an energy resolution of 8×10^{-9} at 14.4 keV. *Rev. Sci. Instrum.* **72**, 4080 (2001).